Electronic Supplementary Material (ESI) for Physical Chemistry Chemical Physics.

Supplementary Information for
"Photogenerated Carrier Dynamics of TIPS-Pentacene Film Analysed through Photocurrent and Electrically Detected Magnetic Resonance"

Ken Kato and Yoshio Teki *

Division of Molecular Materials Science, Graduate School of Science,
Osaka City University, 3-3-138 Sugimoto, Sumiyoshi-ku, Osaka 558-8585, Japan

* Corresponding author: Y. Teki
E-mail: teki@sci.osaka-cu.ac.jp; Fax: +81-6-6605-2559

Microwave power dependence of the linewidth at 80 K

Fig. S1a shows the microwave power dependence of the normalised EDMR spectra. The EDMR spectra were analysed by eqn (5) in the main text. Fig. S1b presents the microwave power dependence of the Gaussian and Lorentzian linewidths of the EDMR spectra. Gaussian and Lorentzian linewidths did not depend on microwave power. From the linewidth (δB = 0.5 mT) of the Lorentzian line shape, the lower limit of the lifetime (τ) of the weakly coupled e–h pair was estimated to be $1/\tau = 8.6 \times 10^7$ s^{-1} ($\tau = 1.16 \times 10^{-8}$ s) using the relationship $\delta B \approx h/g\beta\tau$.

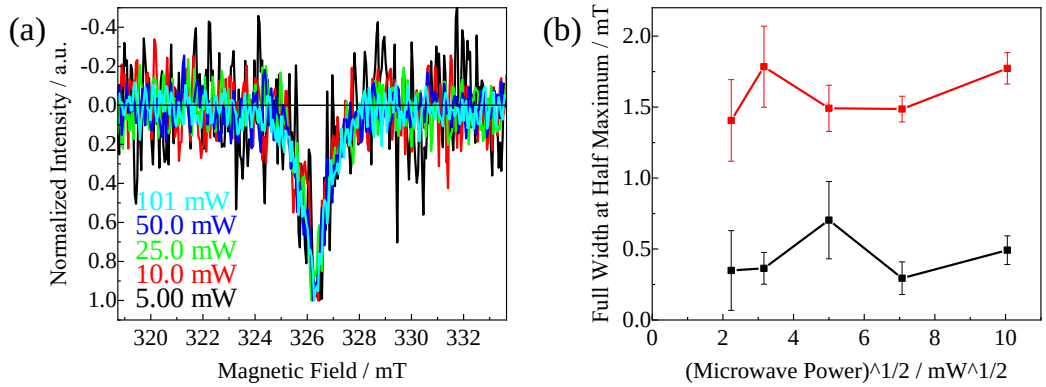

Fig. S1. (a) Microwave power dependence of normalised EDMR spectra of the VVD film of TIPS-Pn under N_2 atmosphere at 80 K. (b) Microwave power dependence of the Gaussian and Lorentzian linewidths.

Cyclic voltammogram

The electrochemical property of TIPS-Pn was studied by cyclic voltammetry in CH_2Cl_2 solution. TIPS-Pn showed a quasi-reversible wave for the redox couple at +0.402 V and −1.448 V vs., ferrocenium/ferrocene (Fc^+/Fc) under identical conditions.

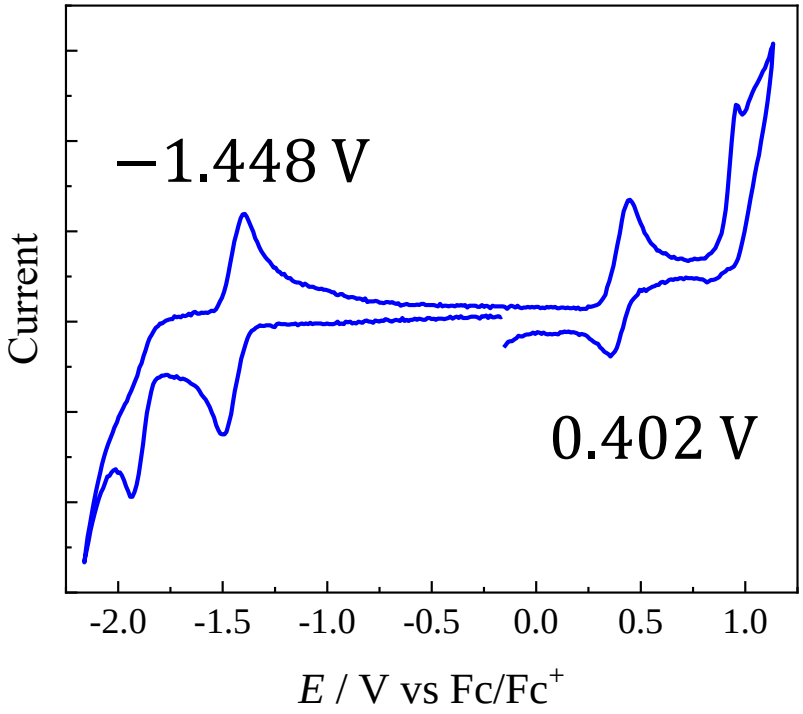

Fig. S2. Cyclic voltammograms of TIPS-Pn in CH_2Cl_2 containing 0.1 M $TBAPF_6$ at room temperature.

Temperature dependence of amplitude for Gaussian and Lorentzian components

Fig. S3 shows the ratio of the amplitude and integral intensity of the Lorentzian to Gaussian component. The amplitude and integral intensity of the Lorentzian component were nearly same as that of the Gaussian component at temperatures below 150 K. However, the contribution of the Lorentzian component decreased as the temperature increased and remained constant at approximately 0.5 at temperatures over 200 K.

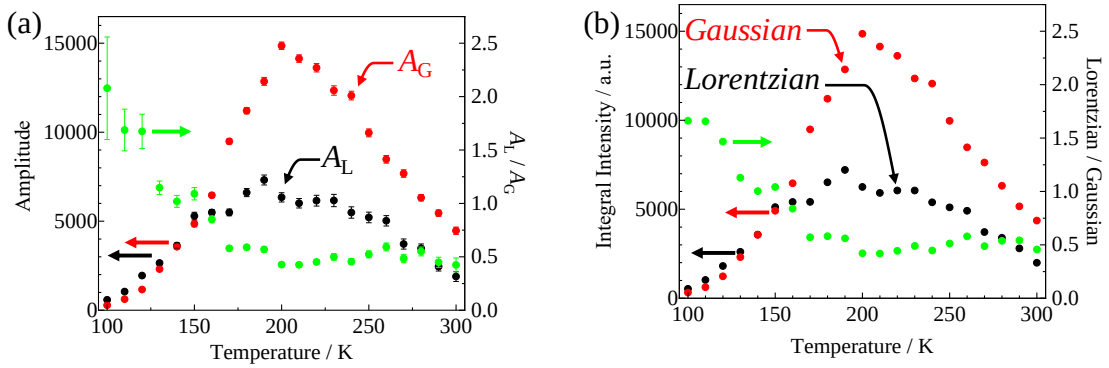

Fig. S3. (a) Temperature dependence of amplitude for Gaussian and Lorentzian components. (b) Temperature dependence of integral intensity for Gaussian and Lorentzian components. The black and red circles show Lorentzian and Gaussian amplitudes, respectively (fitting curves using eqn (5) in the main text).

Analytical solutions of EDMR intensity

S_0-Born Process

The EDMR behaviour could be explained by the carrier generation and deactivation process of the e-h pair, as illustrated in Scheme 1 (Scheme 1 in the main text). The intensity of the EDMR signal is defined as:

$$I_{\mathrm{EDMR}} = I_{\mathrm{on}} - I_{\mathrm{off}} \qquad \text{(S1)}$$

where I_{on} and I_{off} denote the photocurrent intensity in the presence and absence of microwave irradiation, respectively. The photocurrent (I) is given as the sum of the product of the population density (ρ) of the spin sublevels and the dissociative efficiency (k_{dis}).

$$I = \sum_{i}^{S,T_+,T_0,T_-} k_{dis}\rho_i \qquad \text{(S2)}$$

The analytical solution of the EDMR data is derived by solving the simultaneous rate equations of the singlet e-h pairs ^{1}(e-h) and the triplet e-h pairs ^{3}(e-h) shown in Scheme S1. To reproduce the temperature dependence, the dissociative rate constant (k_{dis}) of the carriers from the spin sublevels of ^{1,3}(e-h) pairs was assumed to be a thermally activated process. Thus, the rate constant of carrier generation (k_{dis}) is given by:

$$k_{\mathrm{dis}} = k_0 \exp(-E/k_{\mathrm{B}}T) \qquad \text{(S3)}$$

The rate constants k_{S}, k_{T}, k_{ISC}, and k_{ESR} are independent of the temperature. The population density (ρ) of each spin sublevel under ESR conditions can be obtained by solving eqn (S4).

$$\frac{d\rho_S^{on}}{dt} = I_0 - k_{ISC}\rho_S^{on} - k_{dis}\rho_S^{on} - k_S\rho_S^{on} + k_{ISC}\rho_{T_0}^{on} = 0$$

$$\frac{d\rho_{T_0}^{on}}{dt} = k_{ISC}\rho_S^{on} - k_{ISC}\rho_{T_0}^{on} - 2k_{ESR}\rho_{T_0}^{on} - k_{dis}\rho_{T_0}^{on} - k_T\rho_{T_0}^{on} + k_{ESR}\rho_{T_+}^{on} + k_{ESR}\rho_{T_-}^{on} = 0 \quad \text{(S4)}$$

$$\frac{d\rho_{T_+}^{on}}{dt} = k_{ESR}\rho_{T_0}^{on} - k_{ESR}\rho_{T_+}^{on} - k_{dis}\rho_{T_+}^{on} - k_T\rho_{T_+}^{on} = 0$$

$$\frac{d\rho_{T_-}^{on}}{dt} = k_{ESR}\rho_{T_0}^{on} - k_{ESR}\rho_{T_-}^{on} - k_{dis}\rho_{T_-}^{on} - k_T\rho_{T_-}^{on} = 0$$

The analytical solutions of the densities (ρ_i^{on}) are given as follows:

$$\rho_S = I_0 \frac{k_{ISC}k_{ESR} + (k_{dis} + k_T)(k_{ISC} + 3k_{ESR} + k_{dis} + k_T)}{F + G} \quad \text{(S5)}$$

$$\rho_{T_0} = I_0 \frac{k_{ISC}(k_{ESR} + k_{dis} + k_T)}{F + G} \quad \text{(S6)}$$

$$\rho_{T_+} = \rho_{T_-} = I_0 \frac{k_{ISC}k_{ESR}}{F + G} \quad , \quad \text{(S7)}$$

where

$$F = k_{ISC}(k_{dis} + k_S)(k_{ESR} + k_{dis} + k_T) + 2k_{ESR}(k_{dis} + k_T)(k_{ISC} + k_{dis} + k_S) \quad \text{(S8)}$$

$$G = (k_{dis} + k_T)(k_{ISC} + k_{dis} + k_S)(k_{ESR} + k_{dis} + k_T) \quad \text{(S9)}$$

Substituting eqns (S5) – (S7) into eqn (S2), the photocurrent intensity under resonance conditions is given by

$$I_{\text{on}} = k_{dis}I_0 \frac{4k_{ISC}k_{ESR} + (k_{dis} + k_T)(2k_{ISC} + 3k_{ESR} + k_{dis} + k_T)}{F + G} \quad \text{(S10)}$$

The analytical solutions of the photocurrent intensity and the population density (ρ_i^{off}) of each spin sublevel under non-resonance conditions can be obtained by substituting $k_{ESR} = 0$ to eqns (S5) – (S7):

The analytical solutions of the densities (ρ_i^{off}) are obtained as follows:

$$\rho_S^{off} = I_0 \frac{k_{ISC} + k_{dis} + k_T}{k_{ISC}(k_{dis} + k_S) + k_{ISC}(k_{dis} + k_T) + (k_{dis} + k_S)(k_{dis} + k_T)} \quad \text{(S11)}$$

$$\rho_{T_0}^{off} = I_0 \frac{k_{ISC}}{k_{ISC}(k_{dis} + k_S) + k_{ISC}(k_{dis} + k_T) + (k_{dis} + k_S)(k_{dis} + k_T)} \quad \text{(S12)}$$

$$\rho_{T_+}^{off} = \rho_{T_-}^{off} = 0 \quad \text{(S13)}$$

Substituting eqns (S11) – (S13) into eqn (S2), the photocurrent intensity under resonance conditions is given by

$$I_{off} = k_{dis}I_0 \frac{2k_{ISC} + k_{dis} + k_T}{k_{ISC}(k_{dis} + k_S) + k_{ISC}(k_{dis} + k_T) + (k_{dis} + k_S)(k_{dis} + k_T)} \quad \text{(S14)}$$

In addition, substituting eqns (S10) and (S14) into eqn (S1), the EDMR intensity (I_{EDMR})

can be expressed as

$$I_{\mathrm{EDMR}} = \frac{2I_0 k_{ESR} k_{dis} k_{ISC}^2 (k_S - k_T)}{AC} \quad , \qquad \text{(S15)}$$

where

$$A = (k_T + k_{dis})(k_S + k_{ISC} + k_{dis}) + k_{ISC}(k_S + k_{dis}) \qquad \text{(S16)}$$

and

$$C = k_{ISC}(k_S + k_{dis})(k_{ESR} + k_T + k_{dis}) + (k_S + k_{ISC} + k_{dis})(k_T + k_{dis})(3k_{ESR} + k_T + k_{dis}) \qquad \text{(S17)}$$

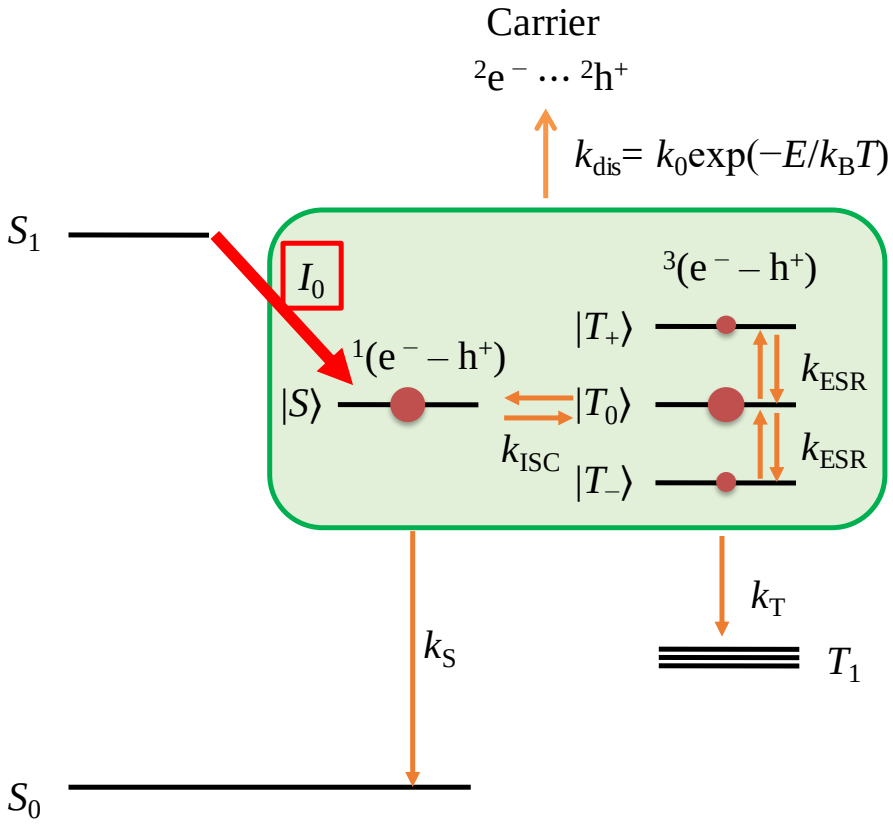

Scheme S1. Excited-state dynamics and carrier generation model in the VVD film of TIPS-Pn.

Fig. S4 shows the temperature dependence of k_{dis}. The maximum intensity of EDMR is obtained when the k_{dis} value is close to those of k_S and k_T, which was achieved at 200 K in the current testing system (Fig. 5 in the main text).

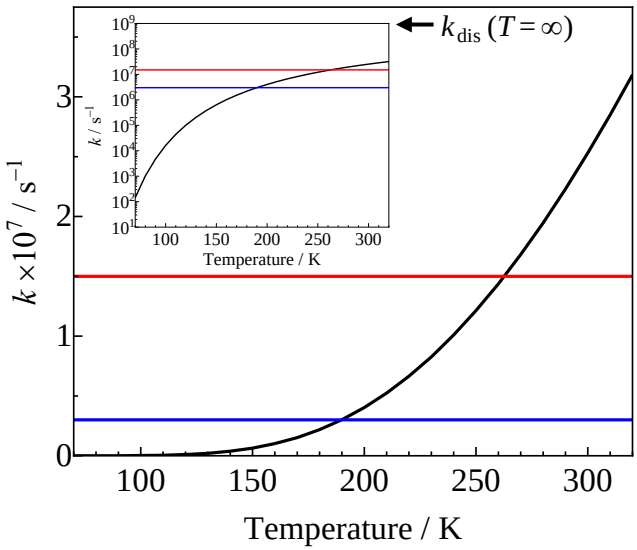

Fig. S4. Temperature dependence of k_{dis} (black curve; $k_0 = 1.0 \times 10^9$ s^{-1}, $E/k_B = 1103$ K). k_S (blue curve; $k_S = 3.0 \times 10^6$ s^{-1}), and k_T (red curve; $k_T = 1.5 \times 10^7$ s^{-1}) are temperature independent rate constants used for the simulation in the main text.

Fig. S5 shows the temperature dependence of the populations (ρ_i) of each spin sublevel. In the non-resonance condition, there is no population of $|T_+\rangle$ and $|T_-\rangle$. However, in the resonant condition, non-zero populations of $|T_+\rangle$ and $|T_-\rangle$ are generated with a decrease in $|S\rangle$ population.

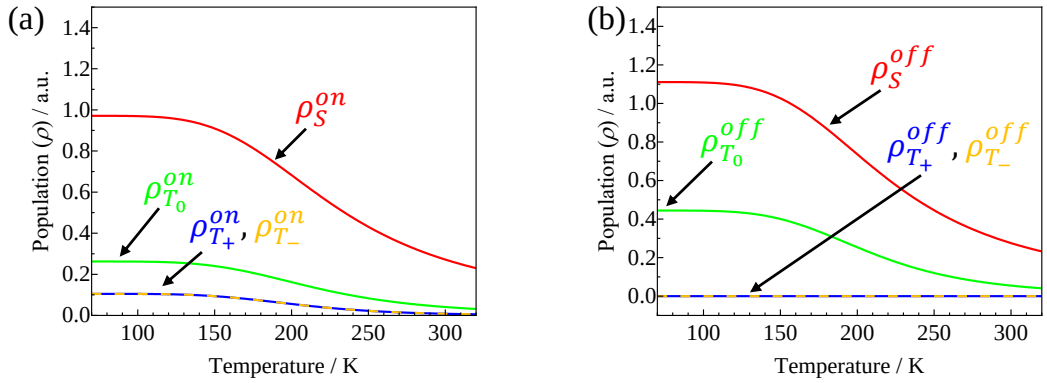

Fig. S5. (a) Temperature dependence of the populations (ρ_i) of each spin sublevel under resonance condition. (b) Temperature dependence under non-resonance condition. In these simulations, $k_S = 3.0 \times 10^6$ s^{-1}, $k_T = 1.5 \times 10^7$ s^{-1}, $k_0 = 1.0 \times 10^9$ s^{-1}, $E/k_B = 1103$ K, $k_{ESR} = 1.0 \times 10^7$ s^{-1}, and $k_{ISC} = 1.0 \times 10^7$ s^{-1} were used.

Fig. S6 shows the E/k_B and k_0 dependence of the EDMR peak. Although the temperature giving the peak position and the temperature width were depended on the k_{dis} parameters (k_0 and E), the maximum intensity was independent of those parameters. The peak temperature was proportional to E/k_B, and not to k_0.

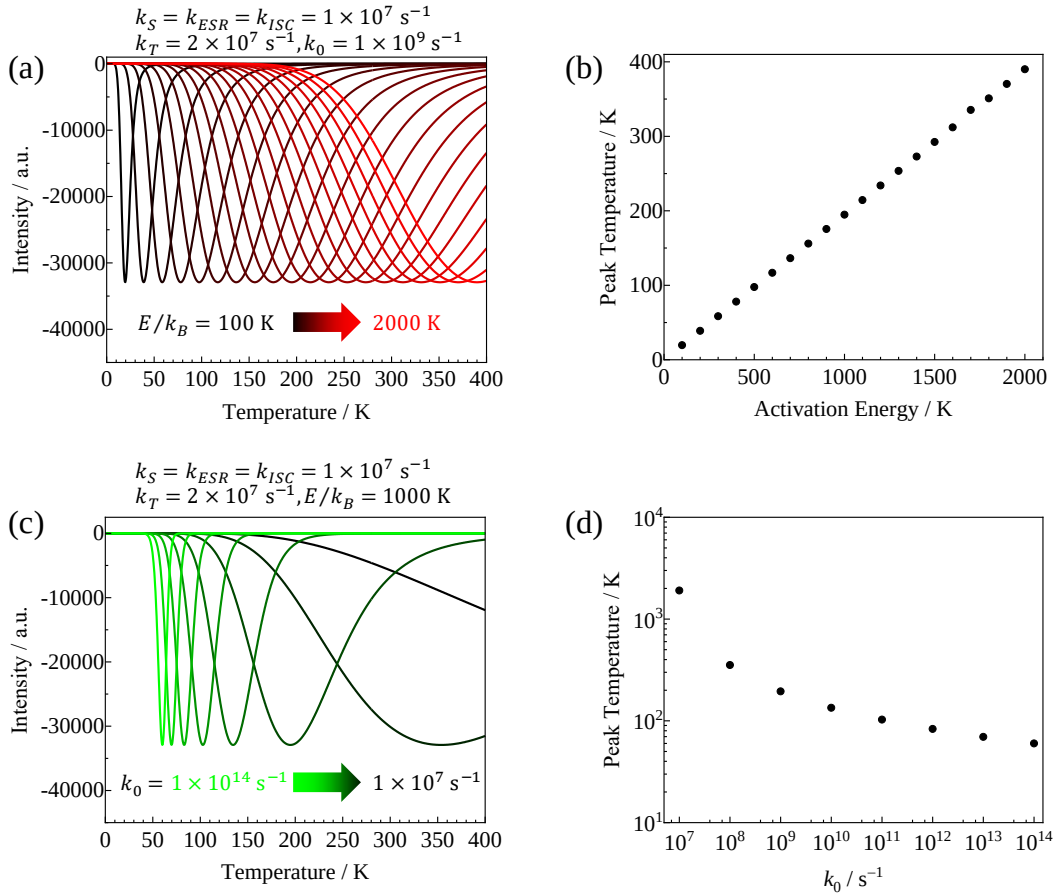

Fig. S6. (a) E/k_B dependence of the EDMR peak and (b) peak temperature vs. activation energy (E/k_B). ($k_S = 1.0 \times 10^7$ s^{-1}, $k_T = 2.0 \times 10^7$ s^{-1}, $k_0 = 1.0 \times 10^9$ s^{-1}, $k_{ESR} = 1.0 \times 10^7$ s^{-1}, $k_{ISC} = 1.0 \times 10^7$ s^{-1}). (c) k_0 dependence of the EDMR behaviour and (d) peak temperature vs. k_0. ($k_S = 1.0 \times 10^7$ s^{-1}, $k_T = 1.4 \times 10^7$ s^{-1}, $E/k_B = 1000$ K, $k_{ESR} = 1.0 \times 10^7$ s^{-1}, $k_{ISC} = 1.0 \times 10^7$ s^{-1}).

Fig. S7 shows the EDMR intensity as a function of the simulated k_T. The analytical solution shows that the sign of the EDRM signal is determined by the difference in the rate constants, ($k_S - k_T$). EDMR was not observed when $k_S = k_T = 0$. The signal is positive when $k_S > k_T$ and negative when $k_S < k_T$. The EDMR intensity was significantly decreased when k_T was sufficiently higher than k_{dis}. The peak position depended on k_T when k_T was close to the other transition rate constants (k_{ISC} and k_{ESR}).

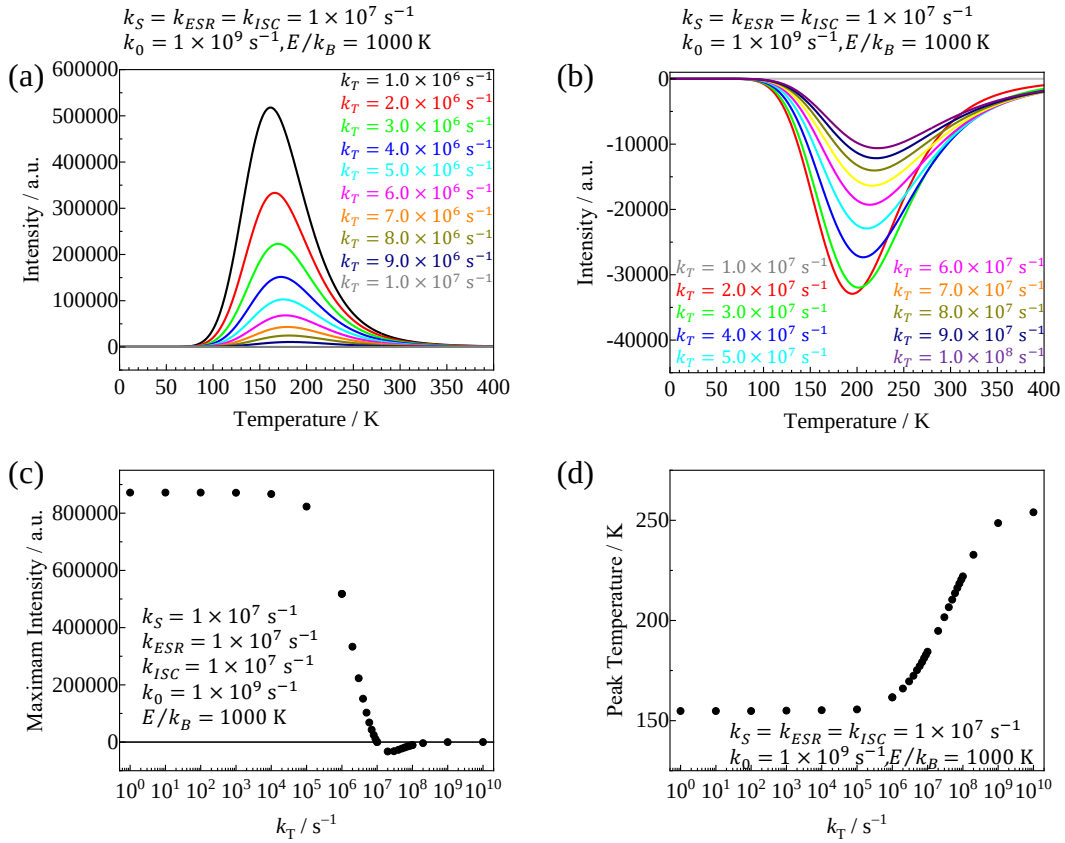

Fig. S7. The k_T dependence of the EDMR behaviour (a) $k_T = 10^6$ to $10^7\ s^{-1}$ and (b) $k_T = 10^7$ to $10^8\ s^{-1}$. (c) Peak temperature vs. k_T. (d) Maximum intensity vs. k_T. ($k_S = 1.0 \times 10^7\ s^{-1}$, $k_0 = 1.0 \times 10^9\ s^{-1}$, $E/k_B = 1000$ K, $k_{ESR} = 1.0 \times 10^7\ s^{-1}$, $k_{ISC} = 1.0 \times 10^7\ s^{-1}$).

Fig. S8 shows the simulated k_{ESR} and k_{ISC} dependence of the EDMR intensity. The temperature dependence of the EDMR peak k_{ESR} is similar to that of k_{ISC}. The peak position depended on k_{ESR} and k_{ISC}, when k_{ESR} and k_{ISC} were close to the other rate constants. The behaviours were quite similar to those presented in Fig. S7d, but a small change was observed. The EDMR signal was not observed when $k_{ESR} = 0$ and/or $k_{ISC} = 0$. The maximum intensity (negative sign) increased monotonically with an increase in k_{ESR} and k_{ISC}.

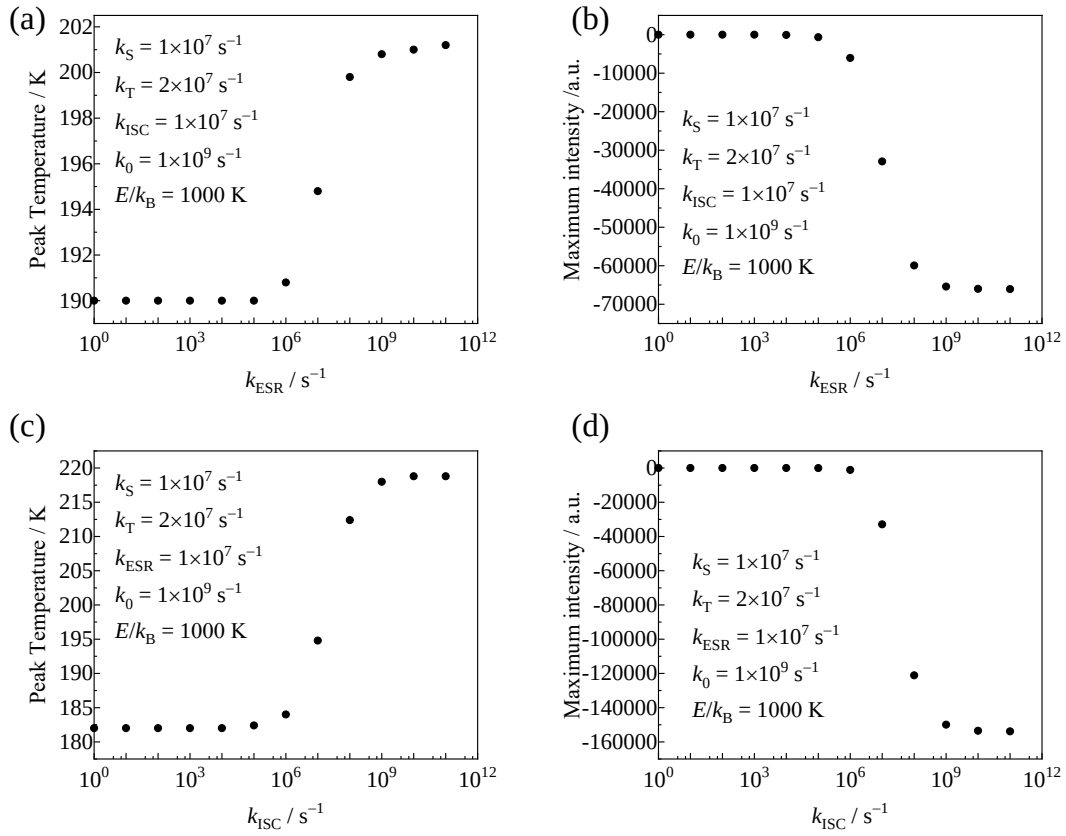

Fig. S8. The k_{ESR} dependence of the EDMR behaviour. (a) Peak temperature vs. k_{ESR}. (b) Maximum intensity vs. k_{ESR}. (k_S = 1.0 × 10^7 s^{-1}, k_T = 2.0 × 10^7 s^{-1}, k_0 =1.0 × 10^9 s^{-1}, E/k_B = 1000 K, k_{ISC} = 1.0 × 10^7 s^{-1}), and the k_{ISC} dependence of the EDMR behaviour. (c) Peak temperature vs. k_{ISC}. (d) Maximum intensity vs. k_{ISC}. (k_S = 1.0 × 10^7 s^{-1}, k_T = 2.0 × 10^7 s^{-1}, k_0 =1.0 × 10^9 s^{-1}, E/k_B = 1000 K, k_{ESR} = 1.0 × 10^7 s^{-1}),

Analytical solutions of EDMR intensity

T$_0$-Born Process

In this study, we assumed the population at $|S\rangle$ from Rehm-Weller's equation. However, herein the analytical solution when the population at $|T_0\rangle$ is solved. The EDMR behaviour can be explained by the carrier generation and deactivation process of the e-h pair, as illustrated in Scheme 2. The intensity of the EDMR signal is defined by eqn (S1).

The analytical solution of the EDMR may be derived by solving the simultaneous rate equations of singlet e-h pairs ^{1}(e-h) and triplet e-h pairs ^{3}(e-h), as shown in Scheme S2. To reproduce the temperature dependence, the dissociative rate constant (k_{dis}) to the carriers from the spin sublevels of ^{1,3}(e-h) pairs was assumed to be a thermally activated process. Thus, the rate constant of carrier generation *(*k_{dis}) is given by eqn (S3).

The population density (ρ) of each spin sublevel under ESR conditions can be obtained by solving the following simultaneous equations.

$$\frac{d\rho_S^{on}}{dt} = -k_{ISC}\rho_S^{on} - k_{dis}\rho_S^{on} - k_S\rho_S^{on} + k_{ISC}\rho_{T_0}^{on} = 0$$

$$\frac{d\rho_{T_0}^{on}}{dt} = I_0 - k_{ISC}\rho_S^{on} - k_{ISC}\rho_{T_0}^{on} - 2k_{ESR}\rho_{T_0}^{on} - k_{dis}\rho_{T_0}^{on} - k_T\rho_{T_0}^{on} + k_{ESR}\rho_{T_+}^{on} + k_{ESR}\rho_{T_-}^{on} = 0$$

$$\frac{d\rho_{T_+}^{on}}{dt} = k_{ESR}\rho_{T_0}^{on} - k_{ESR}\rho_{T_+}^{on} - k_{dis}\rho_{T_+}^{on} - k_T\rho_{T_+}^{on} = 0$$

$$\frac{d\rho_{T_-}^{on}}{dt} = k_{ESR}\rho_{T_0}^{on} + k_{ESR}\rho_{T_-}^{on} - k_{dis}\rho_{T_-}^{on} - k_T\rho_{T_-}^{on} = 0 \qquad \text{(S18)}$$

The analytical solutions of the densities (ρ_i^{on}) are as follows:

$$\rho_S = I_0\frac{k_{ISC}(k_{ESR} + k_{dis} + k_T)}{H + I} \qquad \text{(S19)}$$

$$\rho_{T_0} = I_0\frac{(k_{ISC} + k_{dis} + k_S)(k_{ESR} + k_{dis} + k_T)}{H + I} \qquad \text{(S20)}$$

$$\rho_{T_+} = \rho_{T_-} = I_0\frac{k_{ESR}(k_{ISC} + k_{dis} + k_S)}{H + I} \qquad \text{(S21)}$$

where

$$H = (k_S + k_{ISC} + k_{dis})(k_T + k_{dis})(3k_{ESR} + k_T + k_{dis}) \qquad \text{(S22)}$$

$$I = k_{ISC}(k_S + k_{dis})(k_{ESR} + k_T + k_{dis}) \qquad \text{(S23)}$$

Substituting eqns (S19) –(S21) into eqn (S2), the photocurrent intensity under resonance conditions is given by

$$I_{\text{on}} = k_{dis}I_0\frac{k_{ISC}(k_{ESR} + k_{dis} + k_T) + (k_{ISC} + k_{dis} + k_S)(k_{ESR} + k_{dis} + k_T) + 2k_{ESR}(k_{ISC} + k_{dis} + k_S)}{H + I} \qquad (S24)$$

The analytical solutions of the photocurrent intensity and the population density (ρ_i^{off}) of each spin sublevel under non-resonance conditions are obtained by substituting $k_{ESR} = 0$ to eqns (S19) – (S21).

The analytical solutions of the densities (ρ_i^{off}) are as follows:

$$\rho_S^{off} = I_0\frac{k_{ISC}}{(k_{ISC} + k_{dis} + k_S)(k_{ISC} + k_{dis} + k_T) - k_{ISC}^2} \qquad \text{(S25)}$$

$$\rho_{T_0}^{off} = I_0\frac{k_{ISC} + k_{dis} + k_T}{(k_{ISC} + k_{dis} + k_S)(k_{ISC} + k_{dis} + k_T) - k_{ISC}^2} \qquad \text{(S26)}$$

$$\rho_{T_+}^{off} = \rho_{T_-}^{off} = 0 \qquad \text{(S27)}$$

Substituting eqns (S25) – (S27) into eqn (S2), the photocurrent intensity under resonance

conditions is given by

$$I_{off} = k_{dis} I_0 \frac{2k_{ISC} + k_{dis} + k_T}{(k_{ISC} + k_{dis} + k_S)(k_{ISC} + k_{dis} + k_T) - k_{ISC}^2} \quad \text{(S28)}$$

Substituting eqns (S24) and (S28) into eqn (S1), the EDMR intensity (I_{EDMR}) can be expressed as

$$\begin{aligned} I_{\mathrm{EDMR}} &= I_{\mathrm{on}} - I_{\mathrm{off}} \\ &= \frac{2I_0 k_{ESR} k_{dis} k_{ISC} (k_T - k_S)(k_S + k_{ISC} + k_{dis})}{AC} \end{aligned} \quad \text{(S29)}$$

where A and C are given by eqns (S16) and (S17), respectively.

Using the same parameters, eqn (S29) obtained by distribution in $|T_0\rangle$ has the opposite sign of the signal in eqn (S15) obtained by population in $|S\rangle$.

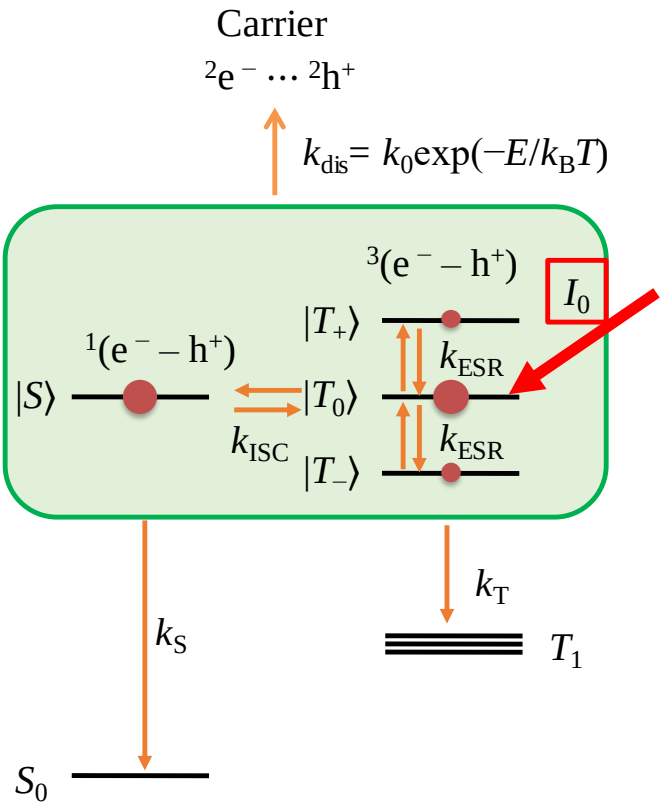

Scheme S2. Excited-state dynamics and carrier generation process in the VVD film of TIPS-Pn.

Detailed procedures for quantum mechanical simulation of EDMR spectra

The EDMR simulation of the kinetic model shown in Scheme S1 is solved by quantum mechanics using the stochastic Liouville equation of the density matrices, which is given by

$$\frac{\mathrm{d}\boldsymbol{\rho}_{eh}}{\mathrm{d}t} = I_0\langle|\boldsymbol{\Lambda}_S|\rangle - \frac{k_{dis}}{2}(\boldsymbol{\rho}_{eh}\boldsymbol{\Lambda}_S + \boldsymbol{\Lambda}_S\boldsymbol{\rho}_{eh}) - \frac{k_{dis}}{2}(\boldsymbol{\rho}_{eh}\boldsymbol{\Lambda}_T + \boldsymbol{\Lambda}_T\boldsymbol{\rho}_{eh}) - \frac{k_S}{2}(\boldsymbol{\rho}_{eh}\boldsymbol{\Lambda}_S + \boldsymbol{\Lambda}_S\boldsymbol{\rho}_{eh}) - \frac{k_T}{2}(\boldsymbol{\rho}_{eh}\boldsymbol{\Lambda}_T + \boldsymbol{\Lambda}_T\boldsymbol{\rho}_{eh}) - \frac{i}{\hbar}[\boldsymbol{H}_{eh} + \boldsymbol{H}_{eh}^{M.W.}, \boldsymbol{\rho}_{eh}] + (Spin\ Relaxation\ Effects), \quad \text{(S30)}$$

$$\boldsymbol{H}_{eh} = \mu_B\boldsymbol{B}\cdot\boldsymbol{g}_e\cdot\boldsymbol{S_e} + \mu_B\boldsymbol{B}\cdot\boldsymbol{g}_h\cdot\boldsymbol{S_h} \quad \text{(S31)}$$

$$\boldsymbol{H}_{eh}^{M.W.} = 2\mu_B\boldsymbol{B_1}\cdot\boldsymbol{g}_e\cdot\boldsymbol{S_e}\cos(\omega t) + 2\mu_B\boldsymbol{B_1}\cdot\boldsymbol{g}_h\cdot\boldsymbol{S_h}\cos(\omega t) \quad \text{(S32)}$$

Here, $\boldsymbol{\rho}_{eh}$ is the density matrix of the e-h pair and the first term, $I_0\langle|\boldsymbol{\Lambda}_S|\rangle$, on the right side denotes the selective population to $|S\rangle$ states from the singlet excited state, $|S_1\rangle$, by continuous photoirradiation. $\boldsymbol{\Lambda}_S$ and $\boldsymbol{\Lambda}_T$ are the projection operators to the singlet and triplet states in the e-h pair, respectively.

$$\boldsymbol{\Lambda}_S = |S><S| \quad \text{(S33)}$$

and

$$\boldsymbol{\Lambda}_T = \sum_i|T_i><T_i| \quad \text{(S34)}$$

Here, $\boldsymbol{H}_{eh}$ and $\boldsymbol{H}_{eh}^{M.W.}$ are the spin Hamiltonian of the e-h pair and that of the interaction with the applied microwave, respectively. $\mu_B\boldsymbol{B}\cdot\boldsymbol{g}_e\cdot\boldsymbol{S_e}$ and $\mu_B\boldsymbol{B}\cdot\boldsymbol{g}_h\cdot\boldsymbol{S_h}$ are the Zeeman interactions with the external magnetic field ($\boldsymbol{B}$). $2\mu_B\boldsymbol{B_1}\cdot\boldsymbol{g}_e\cdot\boldsymbol{S_e}\cos(\omega t)$ and $2\mu_B\boldsymbol{B_1}\cdot\boldsymbol{g}_h\cdot\boldsymbol{S_h}\cos(\omega t)$ are the interactions between the e-h pair and the oscillating microwave with angular frequency (ω). The rate constant of the field-induced radical-pair intersystem crossing (k_{ISC}), which induces S-T_0 mixing, was assumed to occur by the Δg mechanism. It should be noticed that the density matrix and the Hamiltonians depend on θ, ϕ, φ, B, and B_1. Herein, θ, ϕ, and φ are the Eularian angles depicting the rotation of the g tensors from the molecular frame (X, Y, Z) to the laboratory frame (x, y, z) denoted by the external magnetic field (// z-axis) and the microwave field (// x-axis). B and B_1 are the magnetic flux densities of the external static magnetic field and microwave, respectively. In eqns (S30) – (S34), we have chosen the weakly coupled basis representation (WC), in which the basis ket vectors are written as $|S_e, m_e\rangle, |S_h, m_h\rangle$. To calculate the magnetic resonance effect, we performed laboratory frame-to-frame rotating data with the angular frequency (ωt) of the microwave. In the rotating frame, eqn (S30), and the density matrix $\boldsymbol{\rho}_{eh}^{\boldsymbol{rot}}$ can be obtained as follows:

$$\frac{\mathrm{d}\boldsymbol{\rho}_{eh}^{\boldsymbol{rot}}}{\mathrm{d}t} = I_0\langle|\boldsymbol{\Lambda}_S|\rangle - \frac{k_{dis}}{2}(\boldsymbol{\rho}_{eh}^{\boldsymbol{rot}}\boldsymbol{\Lambda}_S + \boldsymbol{\Lambda}_S\boldsymbol{\rho}_{eh}^{\boldsymbol{rot}}) - \frac{k_{dis}}{2}(\boldsymbol{\rho}_{eh}^{\boldsymbol{rot}}\boldsymbol{\Lambda}_T + \boldsymbol{\Lambda}_T\boldsymbol{\rho}_{eh}^{\boldsymbol{rot}})$$
$$- \frac{k_S}{2}(\boldsymbol{\rho}_{eh}^{\boldsymbol{rot}}\boldsymbol{\Lambda}_S + \boldsymbol{\Lambda}_S\boldsymbol{\rho}_{eh}^{\boldsymbol{rot}}) - \frac{k_T}{2}(\boldsymbol{\rho}_{eh}^{\boldsymbol{rot}}\boldsymbol{\Lambda}_T + \boldsymbol{\Lambda}_T\boldsymbol{\rho}_{eh}^{\boldsymbol{rot}})$$
$$- \frac{i}{\hbar}\left[\boldsymbol{H}_{eh}^{\boldsymbol{rot}} + \boldsymbol{H}_{eh}^{M.W.,rot}, \boldsymbol{\rho}_{eh}^{\boldsymbol{rot}}\right]$$
$$+ (Spin\ Relaxation\ Effects), \qquad \text{(S35)}$$

and the spin Hamiltonians are expressed as follows:

$$\boldsymbol{H}_{eh}^{\boldsymbol{rot}} + \boldsymbol{H}_{eh}^{\boldsymbol{MW,rot}} = \boldsymbol{AA} + \boldsymbol{BB}e^{i\omega t} + \boldsymbol{CC}e^{-i\omega t} + \boldsymbol{DD}e^{2i\omega t} + \boldsymbol{EE}e^{-2i\omega t} \qquad \text{(S36)}$$

where $\boldsymbol{AA}$ – $\boldsymbol{EE}$ are given by:

$$\boldsymbol{AA} = (g_{zz}^e\mu_B B_0 - \hbar\omega)S_z^e + \frac{\mu_B B_1}{2}\left\{\left(g_{xx}^e - ig_{xy}^e\right)S_+^e + \left(g_{xx}^e + ig_{xy}^e\right)S_-^e\right\} + (g_{zz}^h\mu_B B_0$$
$$- \hbar\omega)S_z^h + \frac{\mu_B B_1}{2}\left\{\left(g_{xx}^h - ig_{xy}^h\right)S_+^h + \left(g_{xx}^h + ig_{xy}^h\right)S_-^h\right\} \qquad \text{(S37)}$$

$$\boldsymbol{BB} = \frac{\mu_B B_1}{2}\left\{\left(g_{xz}^e - ig_{yz}^e\right)S_+^e + \left(g_{xz}^h - ig_{yz}^h\right)S_+^h\right\} + g_{xz}^e\mu_B B_1 S_z^e + g_{xz}^h\mu_B B_1 S_z^h \qquad \text{(S38)}$$

$$\boldsymbol{CC} = \frac{\mu_B B_1}{2}\left\{\left(g_{xz}^e + ig_{yz}^e\right)S_-^e + \left(g_{xz}^h + ig_{yz}^h\right)S_-^h\right\} + g_{xz}^e\mu_B B_1 S_z^e + g_{xz}^h\mu_B B_1 S_z^h \qquad \text{(S39)}$$

$$\boldsymbol{DD} = \frac{\mu_B B_1}{2}\left\{\left(g_{xx}^e - ig_{xy}^e\right)S_+^e + \left(g_{xx}^h - ig_{xy}^h\right)S_+^h\right\} \qquad \text{(S40)}$$

and

$$\boldsymbol{EE} = \frac{\mu_B B_1}{2}\left\{\left(g_{xx}^e + ig_{xy}^e\right)S_-^e + \left(g_{xx}^h + ig_{xy}^h\right)S_-^h\right\} \qquad \text{(S41)}$$

In the present e-h pairs, the anisotropy of the $\boldsymbol{g}$ tensors is small. Therefore, only the $\boldsymbol{AA}$ term, which is time-independent, will be addressed hereafter because the non-secular terms $\boldsymbol{BB}$, $\boldsymbol{CC}$, $\boldsymbol{DD}$, and $\boldsymbol{EE}$ in (S36) can be neglected.

The rate equation of (S32) was rewritten in the Liouville space as follows:

$$\frac{\mathrm{d}}{\mathrm{d}t}\boldsymbol{\rho}_{eh}^{\boldsymbol{L,rot}} = I_0\langle|\boldsymbol{\Lambda}_S|\rangle - \boldsymbol{L}_{eh}\boldsymbol{\rho}_{eh}^{\boldsymbol{L,rot}} + \boldsymbol{\Gamma}\boldsymbol{\rho}_{eh}^{\boldsymbol{L,rot}} \qquad \text{(S42)}$$

where

$$\boldsymbol{\rho}_{eh}^{\boldsymbol{L,rot}}(t) = \begin{pmatrix} \rho^{rot}(t)_{11} \\ \rho^{rot}(t)_{12} \\ \vdots \end{pmatrix}, \qquad \text{(S43)}$$

and

$$\boldsymbol{L}_{eh} = \frac{k_{dis}}{2}(\boldsymbol{\Lambda_S}\otimes\boldsymbol{E} + \boldsymbol{E}\otimes\boldsymbol{\Lambda_S^*}) + \frac{k_{dis}}{2}(\boldsymbol{\Lambda_T}\otimes\boldsymbol{E} + \boldsymbol{E}\otimes\boldsymbol{\Lambda_T^*}) + \frac{k_S}{2}(\boldsymbol{\Lambda_S}\otimes\boldsymbol{E} + \boldsymbol{E}\otimes\boldsymbol{\Lambda_S^*})$$
$$+ \frac{k_T}{2}(\boldsymbol{\Lambda_T}\otimes\boldsymbol{E} + \boldsymbol{E}\otimes\boldsymbol{\Lambda_T^*}) - \frac{i}{\hbar}(\boldsymbol{AA}\otimes\boldsymbol{E} - \boldsymbol{E}\otimes\boldsymbol{AA}^*) \qquad \text{(S44)}$$

Here, $\boldsymbol{\Gamma}$ is the spin-relaxation matrix and $\boldsymbol{E}$ is the unit matrix. The spin-relaxation matrix in the eigenfunction representation of $\boldsymbol{H}_{eh}$, is expressed by

$$\boldsymbol{\Gamma} = \boldsymbol{\Gamma^{SL}} + \boldsymbol{\Gamma^{PM}} \qquad \text{(S45)}$$

$$\boldsymbol{\Gamma^{SL}} = \frac{1}{T_1}\begin{pmatrix} \frac{1}{Z}\exp\left(-\frac{E_1}{k_B}T\right) & & & & & & & & \\ & 0 & & & & & & & \\ & & 0 & & & & & & \\ & & & 0 & & & & & \\ & & & & \frac{1}{Z}\exp\left(-\frac{E_2}{k_B}T\right) & & & & \\ & & & & & 0 & & & \\ & & & & & & \vdots & & \\ & & & & & & & \vdots & \\ & & & & & & & & \frac{1}{Z}\exp\left(-\frac{E_4}{k_B}T\right) \end{pmatrix}\langle E_{\boldsymbol{L}}| - \frac{1}{T_1}\begin{pmatrix} 1 & 0 & 0 & 0 & 0 & 0 & \cdots & \cdots & 0 \\ 0 & 0 & 0 & 0 & 0 & 0 & \cdots & \cdots & 0 \\ 0 & 0 & 0 & 0 & 0 & 0 & \cdots & \cdots & 0 \\ 0 & 0 & 0 & 0 & 0 & 0 & \cdots & \cdots & 0 \\ 0 & 0 & 0 & 0 & 1 & 0 & \cdots & \cdots & 0 \\ 0 & 0 & 0 & 0 & 0 & 0 & \cdots & \cdots & 0 \\ \vdots & \vdots & \vdots & \vdots & \vdots & \vdots & \ddots & \cdots & \vdots \\ \vdots & \vdots & \vdots & \vdots & \vdots & \vdots & \cdots & \ddots & \vdots \\ 0 & 0 & 0 & 0 & 0 & 0 & \cdots & \cdots & 1 \end{pmatrix} \qquad \text{(S46)}$$

and

$$\boldsymbol{\Gamma^{PM}} = -\frac{1}{T_M}\begin{pmatrix} 0 & 0 & 0 & 0 & 0 & 0 & \cdots & \cdots & 0 \\ 0 & 1 & 0 & 0 & 0 & 0 & \cdots & \cdots & 0 \\ 0 & 0 & 1 & 0 & 0 & 0 & \cdots & \cdots & 0 \\ 0 & 0 & 0 & 1 & 0 & 0 & \cdots & \cdots & 0 \\ 0 & 0 & 0 & 0 & 0 & 0 & \cdots & \cdots & 0 \\ 0 & 0 & 0 & 0 & 0 & 1 & \cdots & \cdots & 0 \\ \vdots & \vdots & \vdots & \vdots & \vdots & \vdots & \ddots & \cdots & \vdots \\ \vdots & \vdots & \vdots & \vdots & \vdots & \vdots & \cdots & \ddots & \vdots \\ 0 & 0 & 0 & 0 & 0 & 0 & \cdots & \cdots & 0 \end{pmatrix} \qquad \text{(S47)}$$

Here, $\boldsymbol{\Gamma^{SL}}$ and $\boldsymbol{\Gamma^{PM}}$ are the spin-lattice relaxation and the phase-relaxation superoperators, respectively, written in the eigenfunction representation. $\langle E_{\boldsymbol{L}}|$ is the row vector representation of $\boldsymbol{E}$ expressed in the Liouville space, which led to $\langle E_{\boldsymbol{L}}|\boldsymbol{\rho}_{eh}^{\boldsymbol{L,rot}} = Tr\{\boldsymbol{\rho}_{eh}^{\boldsymbol{L,rot}}\}$. All operators and density matrices of eqn (S42), which are written in the WC basis representation, were transformed to those in the eigenfunction representation using the unitary transformation matrix, $U_{WC\rightarrow eigen}$ obtained from the eigenfunctions of $\boldsymbol{H}_{eh}$ in the WC basis representation.

In the steady-state approximation of $d\boldsymbol{\rho}_{eh}^{\boldsymbol{L,rot}}/dt = 0$, the solution of the density matrix is given by

$$\boldsymbol{\rho}_{eh}^{L,rot} = I_0(\boldsymbol{L}_{eh} - \boldsymbol{\Gamma})^{-\mathbf{1}}\langle|\boldsymbol{\Lambda}_S|\rangle, \qquad \text{(S48)}$$

The steady-state density matrix of the e-h pairs $\boldsymbol{\rho}_{eh}$ can be obtained directly from $\boldsymbol{\rho}_{eh}^{L,rot}$. The density matrix and the Hamiltonians depend on θ, ϕ, φ, B, and B_1,

although they have been omitted in the above equations. In the current study, EDMR is caused by the change in the efficiency of charge carrier generation from e-h pairs. The efficiency, in which the external magnetic field is applied to the (θ, ϕ) direction in the principal axes (X, Y, Z), can be expressed as follows:

$$\emptyset(\theta, \phi, \varphi, B, B_1) = (k_{dis}/I_0)Tr\{\boldsymbol{\rho}_{eh}(\theta, \phi, \varphi, B, B_1)\} \quad \text{(S49)}$$

Since the molecules are oriented randomly in the sample, the averaged efficiency is given by

$$\langle\emptyset(B, B_1)\rangle = \frac{1}{V}\int_0^{\pi}\int_0^{2\pi}\int_0^{\pi}\emptyset(\theta, \phi, \varphi, B, B_1)\sin\theta \, \mathrm{d}\theta\mathrm{d}\phi\mathrm{d}\varphi \quad \text{(S50)}$$

The relative intensity of the EDMR for the photocurrent intensity can be calculated using the averaged efficiency as follows:

$$I_{\mathrm{EDMR}} = \frac{\langle\emptyset(B, B_1)\rangle - \langle\emptyset(B, 0)\rangle}{\langle\emptyset(B, 0)\rangle} \quad . \quad \text{(S51)}$$

which can be used to compare the simulation and the observed EDMR intensity (1.3%), as shown in Fig. 5a (inset). The simulation curve in Fig. 5b in the main text was calculated using

$$I_{\mathrm{EDMR}} \propto I_0\langle\emptyset(B, B_1)\rangle - \langle\emptyset(B, 0)\rangle \quad . \quad \text{(S52)}$$

The curve in Fig. 5b was obtained for the maximum intensity of the spectra simulated by eqn (52).

Fig. S9 shows the simulated Δg dependence of the EDMR behaviour by the quantum mechanical simulation. For slight differences in g-values, the EDMR behaviour was almost identical.

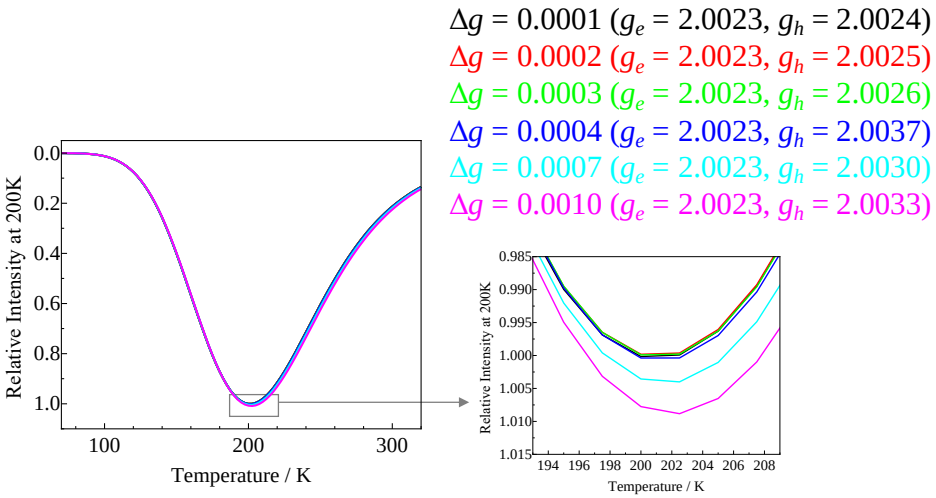

Fig. S9. The Δg dependence of the EDMR behaviour. ($k_S = 3.0 \times 10^6\ s^{-1}$, $k_T = 1.5 \times 10^7\ s^{-1}$, $k_0 = 1.0 \times 10^9\ s^{-1}$, $E/k_B = 1103$ K, and $B_1 = 0.050$ mT.)

Fig. S10 shows the simulated B_1 dependence of the EDMR behaviour by the quantum mechanical simulation.

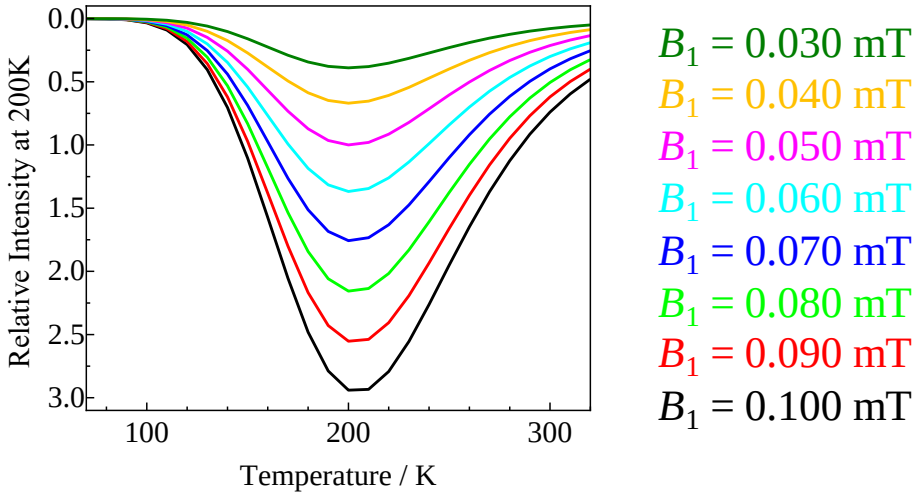

Fig. S10. The B_1 dependence of the EDMR behaviour. ($k_S = 3.0 \times 10^6\ s^{-1}$, $k_T = 1.5 \times 10^7\ s^{-1}$, $k_0 = 1.0 \times 10^9\ s^{-1}$, $E/k_B = 1103$ K, $g_e = 2.0023$ and $g_h = 2.0025$)

Photograph and atomic force microscope (AFM) image

Fig. S11 and **Fig. S12** show the photograph and AFM image of TIPS-Pn VVD film, respectively. DFM mode was used for the measurement and the measurement area was 1 μm x 1 μm (512 pixels in each direction). The scan speed was 0.5 Hz (one scan line in 2 seconds). AFM measurements show that the film has a relative roughness of about 200 nm and is composed of aggregated microcrystals.

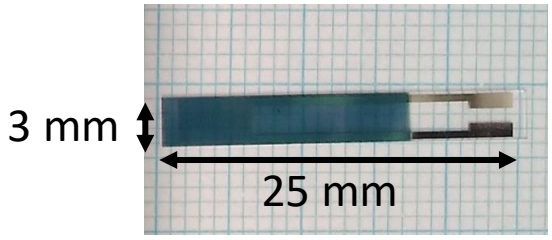

Fig. S11. Photograph of TIPS-Pn VVD film.

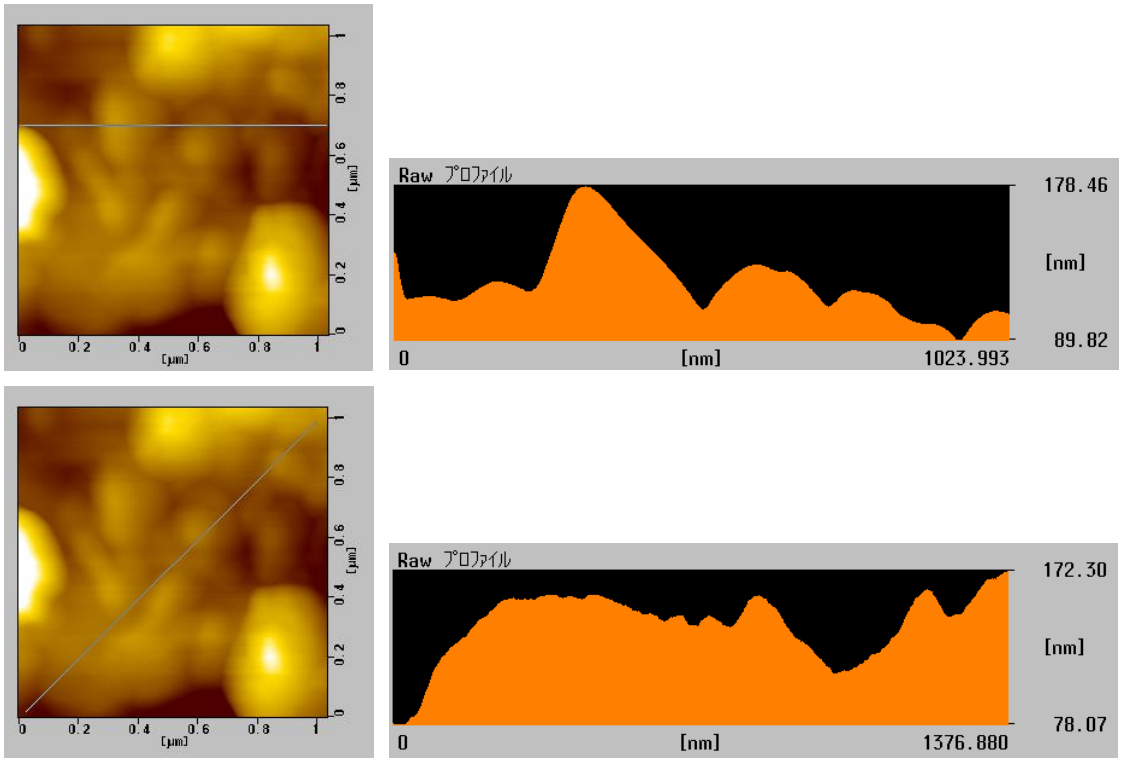

Fig. S12. AFM image of TIPS-Pn VVD film.

Estimation of reorganization energy by the Marcus theory

The schematic diagram showing the charge-separation process followed by the charge hopping transfer is depicted in Fig. S13. Since the Marcus theory is based on the perturbation treatment, it is unclear whether the theory can be applicable straightforwardly to the charge separation between the adjacent π-conjugated molecules with the direct overlap of the π orbitals. However, the following discussions are provided based on the Marcus theory. According to the Marcus theory,[1, 2] the activation energy ($\Delta G^{\dagger}$) is related to the reorganization energy λ and the energy deference (ΔG^{0}) between the reactant and product as follows;

$$\Delta G^{\dagger} = \frac{(\lambda + \Delta G^{0})^{2}}{4\lambda}$$

Therefore, the reorganization energy λ is given by

$$\lambda = \frac{-2(\Delta G^{0} - 2\Delta G^{\dagger}) \pm \sqrt{(\Delta G^{0} - 2\Delta G^{\dagger})^{2} - 4(\Delta G^{0})^{2}}}{2} \quad .$$

When the ΔG^{0} is almost zero, ($\Delta G^{0} \sim 0$), it was approximated as follows;

$$\lambda = 4\Delta G^{\dagger} \text{ (normal region) or } \lambda = 0 \text{ (no barrier)}$$

The reorientation energy λ can be written as the sum of the intramolecular reorganization energy λ_V and the environment reorganization energy λ_S as follows;[3]

$$\lambda = \lambda_V + \lambda_S$$

Here, we consider the following two cases. One is the case that the activation energy (ΔE) estimated by our experiments corresponds to $\Delta G_0^{\dagger}$ on the initial charge separation process. The other one is the case that the estimated activation energy corresponds to $\Delta G_i^{\dagger}$ on the charge hopping process.

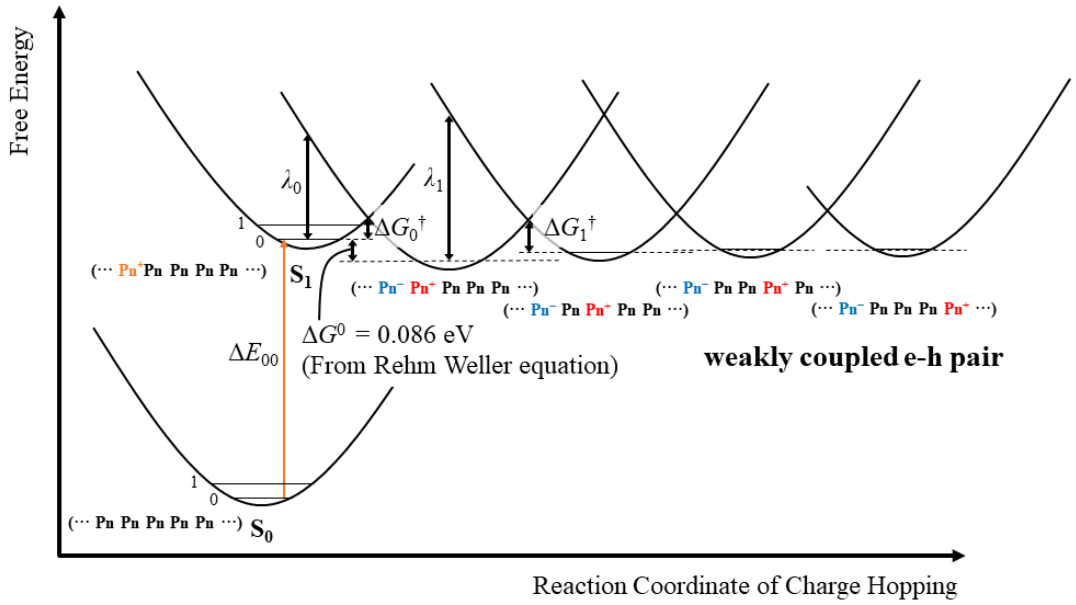

Fig. S13. Energy diagram of excited state, e-h pair and carrier generation process

Case 1: ΔE corresponding to the $\Delta G_0^\dagger$ of charge separation process

In the charge separation process (Pn* + Pn $\rightarrow$ $Pn^+ + Pn^-$), $\Delta G^0 = -0.086$ eV in the main text. Therefore, if the activation energy determined by the temperature dependence of the photocurrent corresponds to $\Delta G_0^\dagger$ ($\Delta G_0^\dagger \sim \Delta E$), the intramolecular reorganization energy due to the charge separation ($S_1 \rightarrow$ (e - h)), λ_0, is given by $\lambda_0 =$ 0.16 eV or 0.046 eV (inverted region). In this case, Scheme S1 (Scheme 1 in the main text) is modified as k_{dis} is independent of the temperature ($k_{dis} = k_0$) and I_0 depends on the temperature;

$$I_0 = I_C \exp(-E/k_B T).$$

Using eqns (2) and (8) in the main text, the temperature dependence of the photocurrent and EDMR intensity were simulated as shown in Fig. S14(a) and S14(b), respectively. The photocurrent was increased as increasing temperature and the observed behavior of the photocurrent can be reproduced. However, the EDMR behavior could not be simulated. Therefore, this result shows that ΔE is not corresponding to the $\Delta G_0^\dagger$ of charge separation process.

Case 2: ΔE corresponding to the $\Delta G^\dagger$ of the charge hopping process

In the charge hopping process (Pn^-Pn^+ Pn Pn··· $\rightarrow$ Pn^-Pn Pn^+ Pn···$\rightarrow\rightarrow\rightarrow$ Pn^-Pn Pn···Pn^+), it is expected to $\Delta G^0 \sim 0$ because of the small Coulomb interaction between Pn^- and Pn^+. If the activation energy determined by the temperature dependence of the

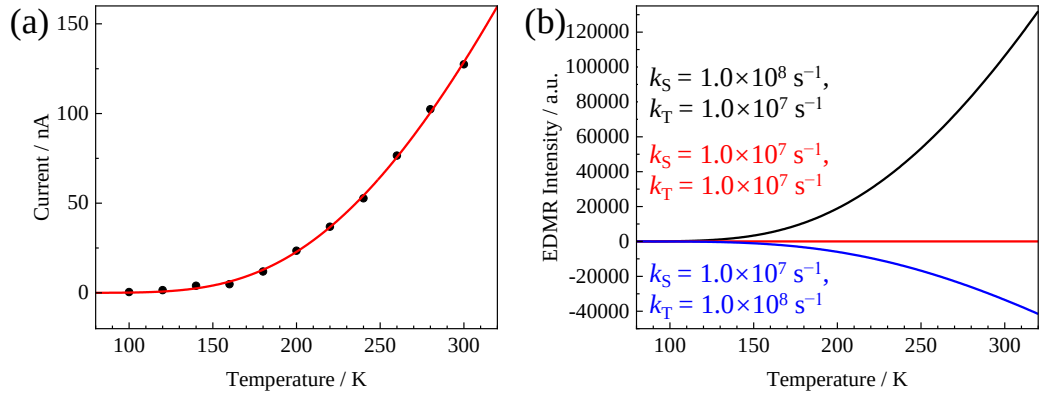

Fig. S14. (a)Photocurrent behavior. (b) EDMR behavior. (k_0 = 1.0 × 10^9 s^{-1}, E/k_B = 1000 K, k_{dis} = k_{ESR} = k_{ISC} = 1.0 × 10^7 s^{-1}).

photocurrent corresponds to $\Delta G^{\dagger}$ in the Marcus theory, $(\Delta G_1^{\dagger} \sim \Delta E)$, $\lambda_1 = 4\Delta G^{\dagger} = 0.3802$ eV (4412 K). The intramolecular reorganization energy due to hole transfer ($Pn^{+}\cdots Pn \rightarrow Pn\cdots Pn^{+}$) of TIPS-Pn is determined by photoelectron spectroscopy in the gas phase as $\lambda_V = 0.111$eV .[4] Since the environment reorientation is negligible in the gas phase, the deference (λ_1-λ_V) leads to the environment reorientation energy λ_S in the solid or liquid phase. Thus, the reorientation energy in a solid-phase medium was estimated as $\lambda_S = 0.269$ eV. In the present experiment, the conduction by electron (anion species) occurs simultaneously in addition to the hole transfer. Therefore, this contribution should be contained into the observed activation energy and λ_S. The carrier hopping is a multistep process as shown in Fig.S13. In this case, the activation energy is not strictly the energy of the carrier generation from the weakly coupled (e - h) pair but corresponds to the activation energy of the carrier hopping.

The result of the EDMR study can be well explained as the activation energy corresponding to the carrier hopping process (the carrier generation process) from the weakly coupled (e-h) pair. Therefore, the case (2) is more appropriate.

1. R. A. Marcus, *J. Chem. Phys*. 1956, 24, 966.
2. R. A. Marcus, *J. Chem. Phys*. 1957, 26, 867.
3. G. J. Kavarnos, and N. J. Turro, *Chem. Rev*. 1986, 86, 401-449.
4. O. L. Griffith, N. E. Gruhn, J. E. Anthony, B. Purushothaman, and D. L. Lichtenberger, *J. Phys. Chem. C* 2008, 112, 20518–20524.